J6.5 SAHARAN DUST AND OPTICAL PROPERTIES OF ANVIL-CIRRUS CLOUDS

Gustavo Carrió, S. C. Van der Heever and W. R. Cotton
Colorado State University, Fort Collins, Colorado

1. INTRODUCTION

High concentrations of Saharan dust have been observed over the peninsula of Florida during CRYSTAL-FACE field campaign held during July 2002. Van der Heever et al. (2004) analyzed the impact of the enhanced concentrations of cloud condensation and ice forming nuclei (CCN and IFN) on the characteristics of convective storms. Their mesoscale simulations indicated that for sensitivity experiments that enhanced cloud forming aerosol, even when area coverage of anvil-cirrus clouds was slightly lower (~3%) although these cloud were significantly thicker

The present study focuses on the potential impact of Saharan dust intrusions on the microphysical structure and optical properties of anvil-cirrus clouds. We performed a series on Large Eddy Simulations (LES) using the Regional Atmospheric Modeling System at Colorado State University (RAMS@CSU). Each numerical experiment was initialized with microphysical and thermodynamic profiles of the above-mentioned mesoscale simulations, corresponding to the time the cirrus-anvil cloud detached from the storm outflow. The effects of IFN and CCN enhancement on ice-particle size distributions as well as different moments were analyzed as the LES model domain followed the trajectory of the cirrus-anvil cloud. Results indicate that Saharan dust intrusions have an important effect on optical properties of anvil-cirrus clouds, and may have a significant radiative cooling effect.

2. MODEL DESCRIPTION

The model used in this study is the 3-D LES version of RAMS@CSU (Cotton et al., 2003). The radiative transfer model used for this study (Harrington et al., 1999) solves the radiative transfer equations for three gaseous constituents, H_2O, O_3, and CO_2 and the optical effects of the hydrometeor size spectra. Gaseous absorption is calculated with a fast exponential sum-fitting of transmissions method proposed. Lorenz-Mie theory is used to compute the optical properties for water drops, while the theory of Mitchell et al. (1996) is used for non-spherical ice crystals. For each hydrometeor species, the band-averaged values of optical properties are computed for the assumed gamma distribution used in RAMS. The microphysical package (Saleeby and Cotton, 2003) shares the double moment microphysical framework of the previous scheme (Meyers et al.,1997) assuming that hydrometeor size spectra have a gamma distribution function and mass mixing ratio as well as number concentration of the hydrometeor species is predicted. For these study, ice particles were categorized in three species: pristine ice, snow and aggregates. Pristine ice. Pristine ice represents particles that have grown only by vapor diffusion. Snow is defined as larger pristine ice crystals (>100 m), which have grown by vapor deposition and riming, while aggregates are defined as ice particles formed by collision and coalescence of pristine ice, snow or other aggregates.

Corresponding author's address : Gustavo G. Carrió, Atmospheric Science Department, Atmospheric Science Bldg., Colorado State University, Fort Collins CO 80523, USA; e-mail: carrio@atmos.colostate.edu

3. EXPERIMENT DESIGN

This series of LES simulations have been performed in a three-dimensional (3-D) framework. Model domain was 5000m in the horizontal and approximately 17000m in the vertical. A constant horizontal and vertical resolution of 50m between the 10000 and 14000m, and a timestep of 2s were used. Vertical grid spacing gradually increases above and below this layer that contains the cirrus-anvil cloud. The lateral boundary conditions were cyclic and the domain top was a rigid lid. Rayleigh damping was used in the five highest levels of the domain to prevent the reflection of vertically traveling gravity waves off this rigid lid. Non-inertial effects were neglected

All numerical experiments were initialized at 21:00Z July 28 2002 and run for a simulation period of 4h. As mentioned in the introduction, each sensitivity run was initialized using microphysical and thermodynamic profiles provided by the fine grid of the corresponding mesoscale simulation, for the time the cirrus-anvil cloud detaches from the storm outflow. Mesoscale vertical profiles following the anvil-cirrus trajectory were used to provide time evolving boundary conditions to the LES simulations. To take into account these large-scale tendencies we applied a Newtonian relaxation technique (nudging) to the total water mixing ratio, ice-liquid potential temperature, and wind components. Nudging terms affect only the horizontal averages, preserving small-scale features developed in the LES model.

A list of the LES runs that correspond to the results presented in this abstract in given in Table 1.

Table I

EXP	IFN	CCN
control	**clean**	**clean**
A25	**25% obs**	**25% obs**
A50	**50% obs**	**50% obs**
A100	**100% obs**	**100% obs**
I50	**50% obs**	**clean**
I100	**100% obs**	**clean**
C50	**clean**	**50% obs**
C100	**clean**	**100% obs**

4. RESULTS

The evolutions of the cloud-averaged ice water content (IWC) and the number concentration (N_i, that include all ice-phase species) are compared in Fig. 1. for control, A50, and A100 runs. Large differences with respect to the control run can be seen for IWC and N_i. At the beginning of the simulation period, IWC simulated for run A100 is approximately 75% larger than that of the control run. These differences rapidly decrease during the first hours of simulation although they remain approximately constant at the between the third and fourth hour (~20% for A100). This rapid decrease in IWC is associated with a larger mass fraction of aggregates (with larger free fall speeds). Conversely, differences in number concentrations do not vary much in time, remaining above 15 and 30% for experiments A50 and A100, respectively. This is also visible in Fig2 that compares ice particle size distributions for the same set of runs. These distributions were obtained using 5-min outputs of the distributions of pristine ice, snow, and aggregates for every cloudy gridcell. For fourth hour, sensitivity experiments exhibit larger modes corresponding to slightly smaller diameter and with no significant differences in the tail of the distributions.

We have not included figures for runs that only consider enhanced CCN or IFN concentration in this abstract. The results of Figs. 1 and 2 remain valid, for experiments C50 and C100, although, differences with respect to the control in water content and number concentration are slightly smaller than those corresponding to A50 and A100. For the runs I50 and I100, simulated values of IWC and N_i are higher than those of the control run, although differences are smaller and no monotonic behavior was observed.

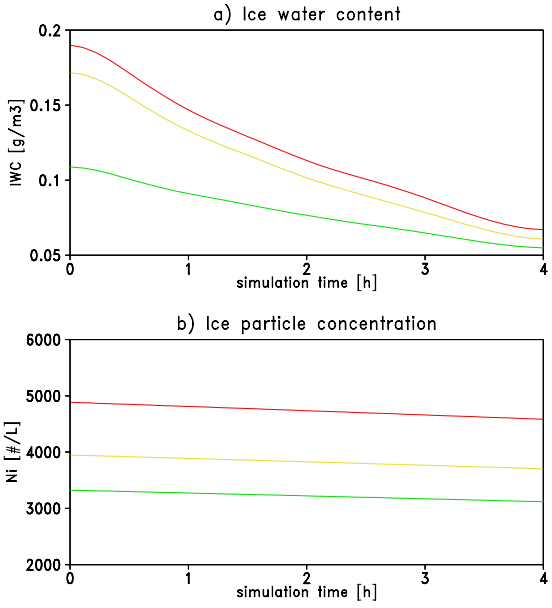

Figure 1. Total ice water content (a). Ice particle concentration (b). Green, yellow, and red lines indicate control, A50, and A100 runs, respectively.

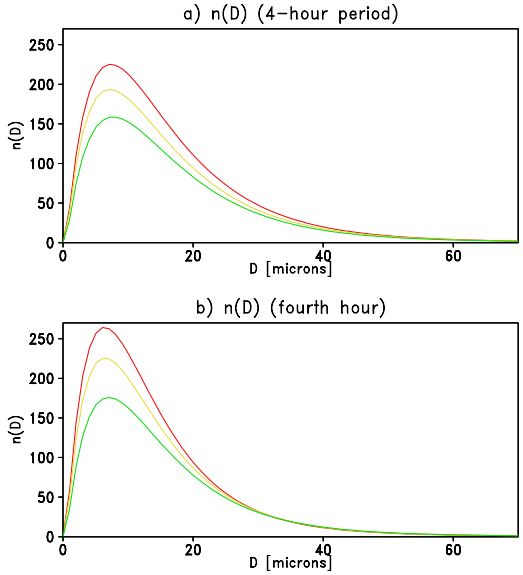

Figure 2. Ice particle size distributions. Green, yellow, and red lines indicate control, A50, and A100 runs, respectively.

Horizontally-averaged vertical profiles of simulated of optical density are compared for the control, A25, A50, and A100 runs, in Figs. 3a, b, c, and d, respectively. During the first two hours, Could base of is lower for sensitivity experiments due to the sedimentation of the larger ice particles. The slightly higher cloud top at the beginning of the simulations is associated with more intense convection in the sensitivity experiments. After the second hour, cloud depth is very similar for all numerical experiments. However, the simulated values oft he optical density are significantly higher. Differences with respect to the control run monotonically increase when considering numerical experiments that correspond to more polluted environments.

The longwave and shortwave downwelling radiative fluxes (LWDN and SWDN) at surface are compared for the control and A100 runs in Fig. 4a and 4b, respectively. Simulated SWDN for experiment A100 is significantly lower (~ -40Wm^{-2}) at the beginning of the simulation period. Differences gradually decrease in absolute value as solar day ends at approximately 3 hours of simulation. Differences in LWDN are smaller (~ 5Wm^{-2}) and opposite in sign.

The time-averaged ratio between the downwelling and upwelling vertical (SWUP) radiative fluxes is plotted as a function of altitude in Fig. 5a.. Simulated cloud reflectivity for run A100 is approximately 10% larger than that of the control run. Cloud reflectivity also shows a monotonical behavior when comparing control run and experiments A25, A50, and A100 (not shown). The simulated turbulent kinetic energy (TKE= u'^2+ v'^2+ w'^2) is compared in Fig 5b. for the control and A100 runs for the 4-h period. Large values of TKE are less frequent for the sensitivity experiment indicating a less turbulent (more stable) cloud.

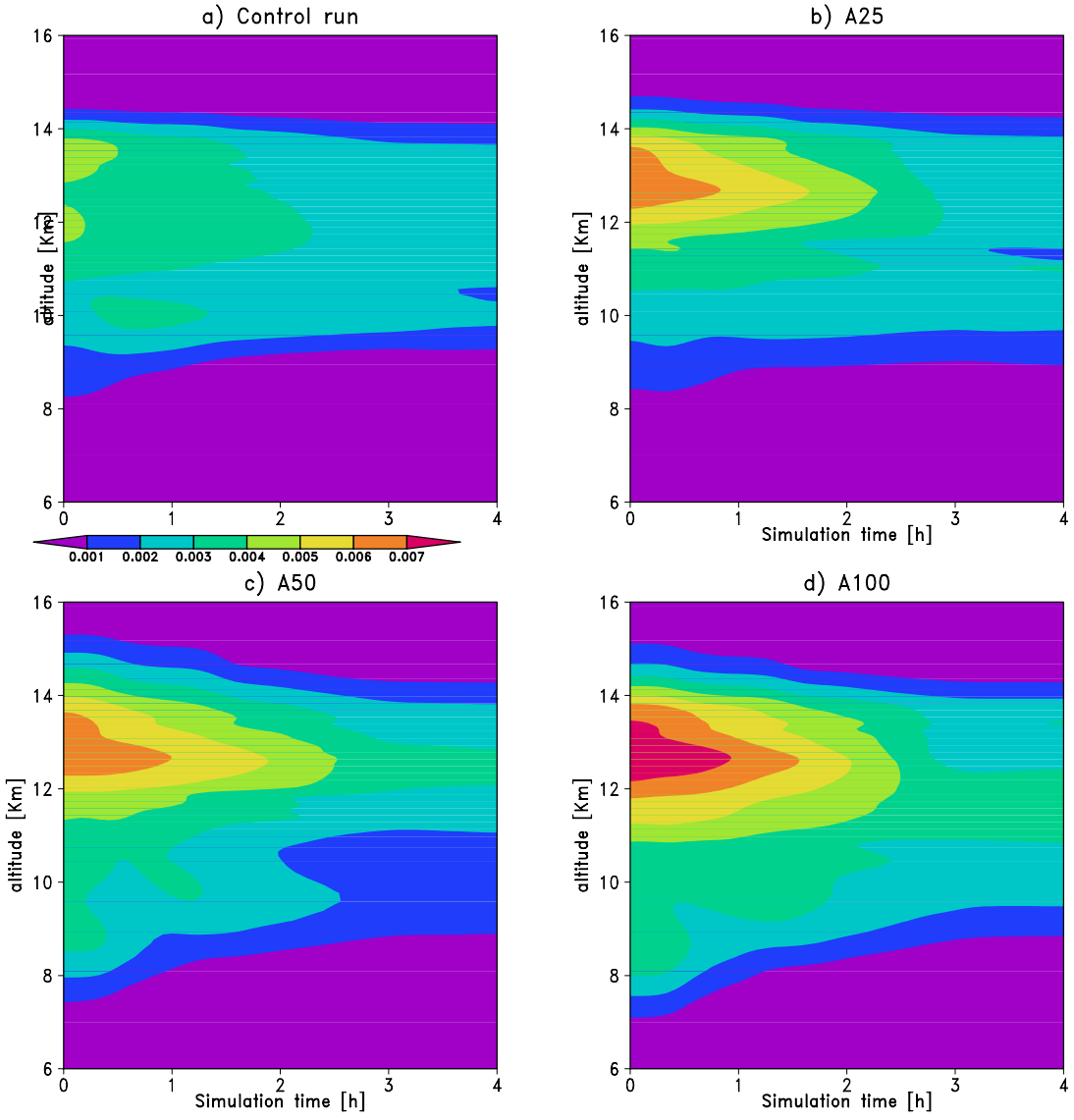

Figure 3. Horizontally-averaged optical density for the control run (a), A25(b), A50(c), and A100(d).

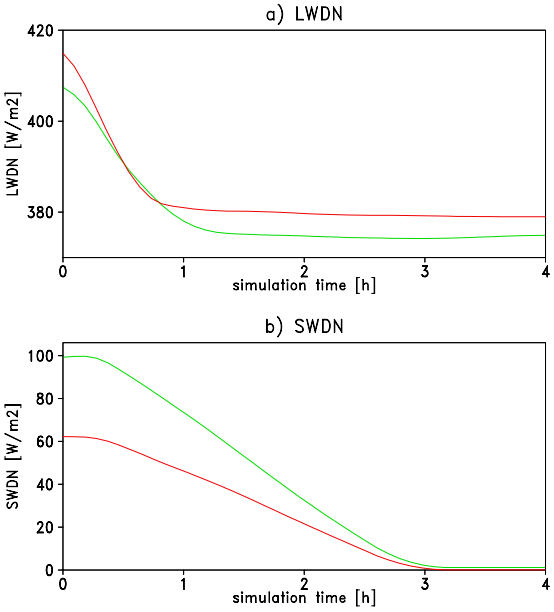

Figure 4. Downwelling radiative fluxes at surface. Green and red solid lines indicate control and A100 runs, respectively.

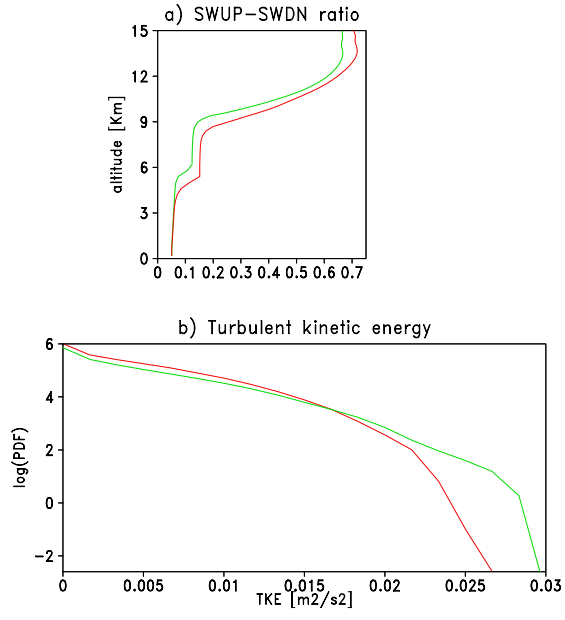

Figure 5. Ratio between upwelling and downwelling radiative fluxes as function of altitude (a). Probability density function of turbulent kinetic energy (b). For both panels, green and red solid lines indicate control and A100 runs, respectively.

The ice particle size distribution obtained for A100, C100, I100 and the control run are compared in Fig. 6. All sensitivity experiments have a significant effect on the distribution. However this figure suggests a less important effect associated with enhancing only IFN concentrations.

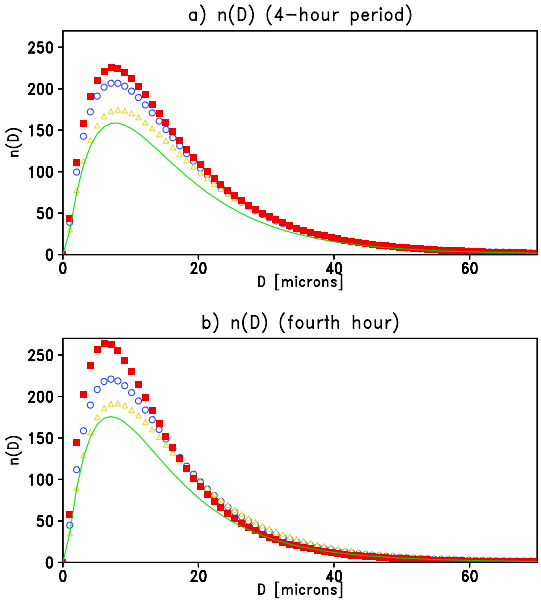

Figure 6. Ice particle size distributions. Solid green line corresponds to the control run, blue circles and yellow triangles indicate runs C100 and I100, respectively. Run A100 is denoted by closed red squares.

We compared the ice particle concentration (0^{th} moment), the mean diameter (ratio between 1^{st} and 0^{th} moments), the effective diameter (~ ratio between 3^{rd} and 2^{nd} moments), and the 2^{nd} moment (proportional to the optical depth) for various runs. Percent differences with respect to the control run are given in Table I for the entire simulation period. The last (shaded) column compares the 4^{th} hour distribution of the control and A100 runs.

Table I Δ% in with respect to the control run

	I100	C100	A25	A50	A100	A100 4th h
M^0	15.8	28.8	5.7	18.1	36.8	33.7
M^1/M^0	4.7	1.1	4.0	-1.6	- 2.7	-8.6
M^3/M^2	0.3	11.0	10.2	18.4	15.6	1.9
M^2	24.6	29.3	16.8	20.7	33.5	13.9

Differences in M^0 and M^2 are most important for the run that corresponds to the observed aerosol concentrations. Enhancing aerosol concentration tend to increase the effective diameter while slightly reducing the mean diameter. Experiment C100 exhibits a similar behavior with a large increase in M^0 and the effective diameter and little (but positive)

change in mean diameter. Conversely, enhancing only IFN concentrations produces larger particles and lower total number concentration. The control run and A100 run exhibit similar evolutions during the last hour of the simulation period. Therefore, the differences for this last hour could be considered a good extrapolation of further evolution.

Horizontally- and temporally-averaged vertical profiles of optical density are given for the control, I100, C100, and A100 runs in Fig. 7..

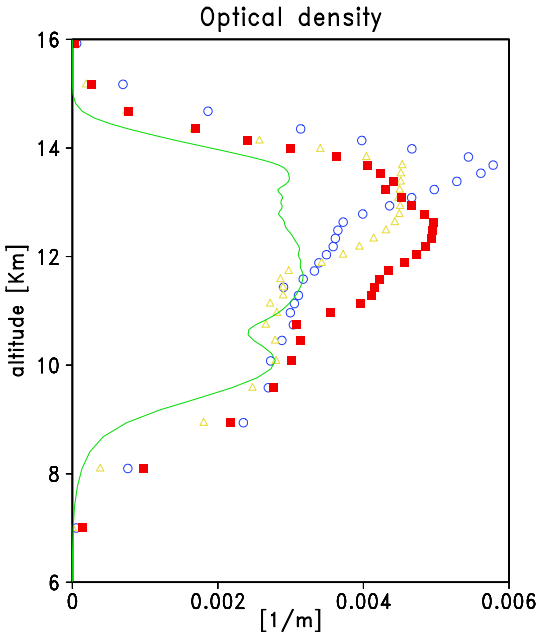

Figure 7. Time-averaged optical density profiles. Solid green line corresponds to the control run, blue circles and yellow triangles indicate runs C100 and I100, respectively. Run A100 is denoted by closed red squares.

The largest maximum corresponds to run C100, although the layer of large optical density is thinner compared to A100. When comparing I100 to A100, it can be seen that the run that only considers IFN enhancement exhibits lmaximum lower in magnitude and vertical depth.

5. CONCLUSIONS

As mentioned in Section 1., we analyzed the impact of Saharan dust intrusion on the characteristics of convective storms in a previous study. Now, we examine the potential effect of these intrusions on the microphysical structure and optical properties of anvil-cirrus clouds. For that purpose, we performed a series on Large Eddy Simulations (LES) following the trajectory of the cirrus-anvil cloud.

Main results can be summarized as follows: For sensitivity experiments, the values of IWC, N_i and optical depth are significantly higher than those of the control run. The largest differences (~40%) in optical depth occur during the first hours of simulation.
Wider size distributions and increased values of effective diameter, number concentration, and optical depth were obtained for numerical experiments that assumed polluted environments. Differences decrease in magnitude and size distributions narrow with time due to the sedimentation of aggregates. Near end of the simulation, A100 and the control run exhibit a similar evolution although, the optical is approximately 14% higher. Conversely, number concentrations of sensitivity experiments remain higher for the entire simulation (~33%).

Both IFN and CCN enhancements show important effects on size distribution. However, results suggest a more important CCN effect as it increases most ice particle concentration while enhancing IFN concentration increases mean diameters. In summary, results suggest that Saharan dust intrusion may have a cooling effect, producing optically thicker cirrus-anvil clouds.

6. ACKNOWLEDGEMENTS

This research was supported by a University of Alaska Fairbanks Research contract UAF-00-0086/FP100092 (CSU 5-33422) and by a NSF grant #0215367. The authors also wish to thank Brenda Thompson for technical support.

7. REFERENCES

Cotton, W. R., R.A. Pielke, Sr., R.L. Walko , G.E. Liston, C.J. Tremback, H. Jiang, R. L. McAnelly, J. Y. Harrington, M.E. Nicholls, G.G. Carrió and J. P. Mc Fadden 2003: RAMS 2001: Current Status and future directions. Meteor. Atmos. Physics, 82, 5-29.

Harrington , Y.Y. , T. Reisin, W.R. Cotton, S. M. Kreidenweis, 1999:Cloud resolving simulations of Arctic stratus. Part II: Transition-season clouds. Atmos. Res., 51, 45-75.

Mitchell, D.L., A. Macke, and Y. Liu, 1996: Modeling cirrus cloudspart II, Treatment of radiative properties. *J. Atmos. Sci.,* **53**, 2967-2988.

Hunke, E. C., and Lipscomb, 1999: CICE: The Los Alamos se-ice model, documentation and software, version 2.0, Los Alamos National Laboratory,LA-CC-98-16, v.2.

Lipscomb, W. H, 2001: Remapping the Thickness Distribution of Sea-ice. J. Geophys. Res..Vol 106, 13989-14000.

Meyers, M. P. Walko, R. L., Harrington J. Y. , Cotton, W.R., 1997: New Rams cloud microphyisics parameterization : Part II. The two-moment scheme. Atmos. Res., 45, 3-39.

Susan C. van den Heever, Carrio, G. G., Cotton, W. R., DeMott, P. J. and A. J. Prenni, 2004: Impacts of nucleating aerosol on Florida convection. Part I: Mesoscale simulations. Submitted to *J. Atmos. Sci.*.